



ChemComm

From lithium to sodium: Design of heterometallic molecular precursors for the NaMO₂ cathode materials

Journal:	<i>ChemComm</i>
Manuscript ID	CC-COM-04-2019-002836.R2
Article Type:	Communication

SCHOLARONE™
Manuscripts



Chemical Communications

COMMUNICATION

From lithium to sodium: Design of heterometallic molecular precursors for the NaMO₂ cathode materials

Received 00th January 20xx,
Accepted 00th January 20xx

Haixiang Han,^{a, c} Zheng Zhou,^a Jesse C. Carozza,^a Jeff Lengyel,^b Yuan Yao,^c Zheng Wei,^a and Evgeny V. Dikarev^{*a}

DOI: 10.1039/x0xx00000x

www.rsc.org/

Based on the well-established model structure of Li₂M₂(tbaaac)₆, the first series of heterometallic molecular precursors Na₂M₂(tbaaac)₆(THF)₂ (M = Fe, Co, and Ni) have been designed and successfully utilized for the preparation of NaMO₂ oxide cathode materials of sodium-ion batteries.

Sodium-ion battery (SIB) cathodes are of great interest to supplement the now-ubiquitous lithium (LIB) analogues, especially for large-scale applications, due to sodium's natural abundance and competitive electrochemistry.¹⁻³ It is well-established that the larger ionic radius of Na⁺ severely limits the number of viable host structures that allow for reversible sodium de/intercalation. The layered sodium–transition metal oxides NaMO₂ represent one of the most promising hosts by providing comparable activity to canonical LIBs.³ This class of compounds can be divided into two major groups, O3 and P2, based on the location of sodium ions at either octahedral or prismatic sites, respectively, squeezed in between the edge-sharing sheets of [MO₆] octahedra.⁴ Current efforts to improve the electrochemical properties of these layered oxides are primarily focused on formation of nanoparticles with highly homogenous metal/vacancy distribution,⁵ and therefore, are intimately tied up to the choice of synthetic strategy.¹

Presently, SIB cathode material preparation is dominated by ball-milling solid state reactions, co-precipitation, sol-gel, and multi-source precursor techniques, which employ physically/chemically incompatible starting reagents that often cause inhomogeneous metal distribution within the target

oxide.⁶⁻¹⁰ Furthermore, the high temperatures required for annealing of these mixtures often result in nanoparticles sintering and agglomerating into larger aggregations, destroying the unique properties brought in by small particle size and specific morphology of materials.^{3,11-13}

The single-source precursor (SSP) approach is the best way to address the above issues as it utilizes molecular complexes containing all necessary elements in the proper ratio and offering low-temperature decomposition pathways to the target functional materials.^{14,15} The intimate mixing of the key elements at the molecular level also provides for a rapid interaction within the heterometallic assembly, effectively preventing the formation of undesired, thermally-stable intermediates.¹⁶ At the same time, the major challenge for the SSP approach remains the design of a suitable molecular complex that features required stoichiometry, clean decomposition pattern, and high solubility in common solvents, while retaining heterometallic structure in solution.¹⁷ Recently-suggested precursors for the Na:M = 1:1 layered oxide materials all have polymeric structures [NaML₃]_∞ (L = acac,⁵ hfac¹³). These compounds are insoluble in non-coordinating solvents, while readily dissociating into homometallic fragments in coordinating ones. Such properties effectively limit precursor feasibility for a number of advanced application techniques, i.e. liquid injection, which is well-known to afford oxide materials in the form of nanoparticles or thin films.

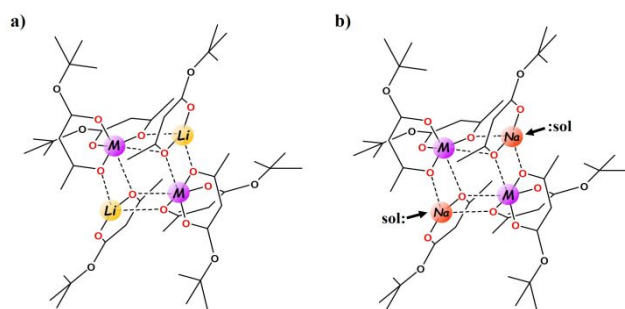
We have previously developed an effective unsymmetric ligand approach to design molecular precursors Li₂M₂L₆ (Scheme 1a; M = transition metal) for the low-temperature preparation of LiMO₂ cathode materials.¹⁵⁻¹⁷ The unsymmetric groups used in the above design feature different (small/bulky) substituents at the two ligand ends. Only the ligand oxygen near the small group is able to participate in both chelating and bridging interactions, while the oxygen under the bulky, sterically-congested end remains purely chelating. The employment of such unsymmetric ligands is effectively changing the connectivity pattern within the heterometallic assembly, allowing for the formation of compounds with

^a Department of Chemistry, University at Albany, State University of New York, 1400 Washington Ave., Albany, NY 12222, USA.

^b Department of Chemistry and Biochemistry, Florida State University, FL 32306, USA.

^c Department of Materials Science and Engineering, Cornell University, NY 14850 USA.

Electronic Supplementary Information (ESI) available: synthetic details, characterization procedures, X-ray powder diffraction patterns, IR and mass spectra, phase analysis of thermal decomposition traces of heterometallic precursors. CCDC 1904470-1904473. For ESI and crystallographic data in CIF or other electronic format, see DOI:10.1039/x0xx00000x

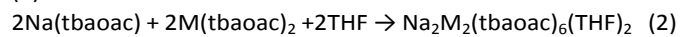
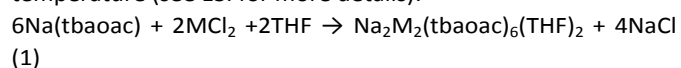


Scheme 1. Design of Na:M = 1:1 molecular precursor based on the model structure of Li analogue.

discrete molecular structures.¹⁷ Among several unsymmetric ligands employed, *tbaoac* (*tert*-butyl acetoacetate) exhibits superior properties such as the lowest decomposition temperature leading to the phase-pure target product as well as the miniscule contribution of the ligand cost to the target material production, thus making the above SSP approach attractive for large-scale applications.¹⁷

The tetranuclear structure of $\text{Li}_2\text{M}_2(\text{tbaoac})_6$ depicted in the Scheme 1a contains tetrahedrally-coordinated Li ions.^{16,17,18} Based on our prior experience, such a model is unlikely suitable for the analogous sodium-containing complex, since Na ion usually commands higher coordination numbers of five or six. We envisaged that it would require an additional neutral donor ligand to satisfy the Na coordination environment (Scheme 1b). Herein, we employ the unsymmetric, inexpensive *tbaoac* ligand along with the strong O-donor THF to design the first family of heterometallic Na:M = 1:1 molecular precursors $\text{Na}_2\text{M}_2(\text{tbaoac})_6(\text{THF})_2$

The heterometallic precursors $\text{Na}_2\text{M}_2(\text{tbaoac})_6(\text{THF})_2$ (M = Fe (**1**), Co (**2**), Ni (**3**), Mg (**4**)) have been prepared in coordinating solvents on a large scale, in nearly quantitative yield using commercially/readily available starting reagents through the following synthetic procedures performed at room temperature (see ESI for more details):



The reactions (1) and (2) were performed in THF, which acts as both reagent and reaction medium. Even though method (2) yields $\text{Na}_2\text{M}_2(\text{tbaoac})_6(\text{THF})_2$ as a sole product, it requires prior preparation of $\text{M}(\text{tbaoac})_2$ as an extra step.

Heterometallic precursors **1–4** appear as fine powders in the colors of orange, pink, green, and white, respectively. Compounds **1** and **2** are relatively sensitive in solution, with air-exposure resulting in a color change to dark-red and green, respectively, indicating the oxidation of divalent iron and cobalt. At the same time, **1** and **2** are stable in the solid state for a reasonable period of time. Compounds **3** and **4** are stable in both solution and the solid state. Heterometallic precursors are soluble in all common solvents. The dissociation of THF from **1–4** takes place at the temperatures above 60 °C, accompanied by a dramatic change in their powder X-ray diffraction patterns.

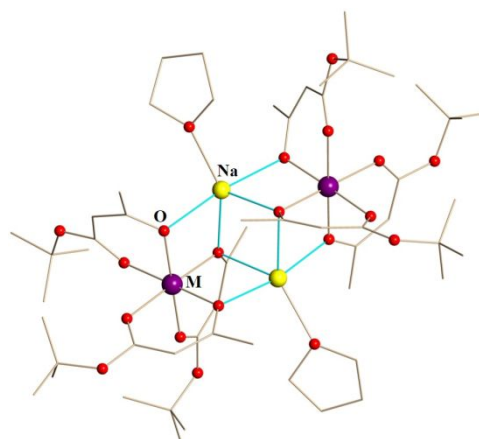


Fig. 1 Molecular structure of $\text{Na}_2\text{M}_2(\text{tbaoac})_6(\text{THF})_2$ (M = Fe, Co, Ni, Mg; Δ, Δ -enantiomer). The sodium–oxygen bonds to the *tbaoac* ligands involved in the bridging interactions are shown in blue. Hydrogen atoms are omitted for clarity. The structural views with thermal ellipsoids can be found in ESI, Figures S5–S8.

Single crystal X-ray diffraction analysis revealed that precursors **1–4** are all isomorphous and crystallize in the centrosymmetric triclinic crystal system. The crystal structure consists of tetranuclear heterometallic molecules (Fig. 1) with Na:M ratio of 1:1. Two transition metal centers bear three chelating *tbaoac* ligands each, exhibiting a distorted octahedral coordination environment. The sodium centers are 5-coordinate with four bridging oxygens coming from the *tbaoac* ligands and one from THF molecule. Molecular structures **1–4** feature six bulky O^tBu groups facing outward of heterometallic assembly and, along with two THFs, providing a screening protection for the metal cores from being engaged in intermolecular interactions that could result in oligomerization and formation of polymeric chains. The averaged metal–oxygen bond lengths in the structures of heterometallic precursors **1–4** (Table 1) show a trend that corresponds well with the radii of divalent Fe, Co, Ni, and Mg ions. While the chelating-bridging M–O distances appear to be somewhat shorter than the chelating ones, a similar situation has been observed previously for the $\text{Li}_2\text{M}_2(\text{tbaoac})_6$ system.¹⁶

Despite certain compositional and structural similarities between the two families of heterometallic precursors $\text{Li}_2\text{M}_2(\text{tbaoac})_6$ and $\text{Na}_2\text{M}_2(\text{tbaoac})_6(\text{THF})_2$, they appear to be different in many aspects. Specifically, the latter is featuring 5-

Table 1 Averaged metal–oxygen bond lengths (Å) in the structures of heterometallic precursors **1–4** (L = *tbaoac*). The full list of bond distances and angles can be found in ESI, Tables S10–S13

	M–O ^c	M–O ^{c,b}	Na–O ^{b,c}	Na–O ^{THF}
$\text{Na}_2\text{Fe}_2\text{L}_6(\text{THF})_2$ (1)	2.103(1)	2.084(1)	2.361(2)	2.358(2)
$\text{Na}_2\text{Co}_2\text{L}_6(\text{THF})_2$ (2)	2.072(1)	2.061(1)	2.351(2)	2.356(2)
$\text{Na}_2\text{Ni}_2\text{L}_6(\text{THF})_2$ (3)	2.038(1)	2.031(1)	2.351(2)	2.357(2)
$\text{Na}_2\text{Mg}_2\text{L}_6(\text{THF})_2$ (4)	2.051(2)	2.051(2)	2.366(2)	2.360(2)

^ac – chelating, ^bc-b – chelating–bridging. ^cc – bridging

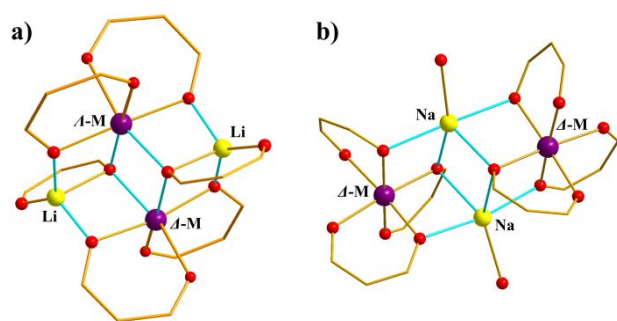


Fig. 2 Tetranuclear cores $[A_2M_2L_6]$ ($A = \text{Li}$ (a) and Na (b); $L = \text{tbaoc}$) representing different connectivity patterns within heterometallic assemblies as well as different chiralities of transition metal centers.

coordinated alkali metals in addition to all ligands chelating transition metal ions. That results in distinctively different heterometallic tetranuclear cores as shown in Figure 2. Another notable difference is that $\text{Li}_2\text{M}_2(\text{tbaoc})_6$ molecule (Fig. 2a) has an inversion center in the middle of heterometallic assembly, making two transition metal centers to display the opposite Δ/Λ -chiralities. Conversely, the $\text{Na}_2\text{M}_2(\text{tbaoc})_6$ core (Fig. 2b) does not contain any extra crystallographic symmetry and features its transition metals in either Δ,Δ - or Λ,Λ -configurations. However vaguely, the latter represents an alternative connectivity pattern within the tetranuclear cyclic assembly by which a diastereomer to the lithium counterpart can be constructed.

The ^1H NMR investigation of compounds **1–3** in chloroform, acetone, and THF revealed signal-silent spectra, indirectly confirming the retention of heterometallic structures in solution. The diamagnetic analog $\text{Na}_2\text{Mg}_2(\text{tbaoc})_6(\text{THF})_2$ (**4**) has been specifically isolated to assess the solution behavior of heterometallic core by NMR spectroscopy. The ^1H NMR spectrum of **4** in chloroform displays three singlets that correspond to tbaoc ligand protons in addition to two signals of coordinated THF molecules (Fig. 3; ESI, Fig. S13 and Table S14), thus confirming that heterometallic structure remains intact upon dissolution.

The “gas-phase structure” of heterometallic precursors **1–3** has been investigated by Direct Analysis in Real Time (DART)

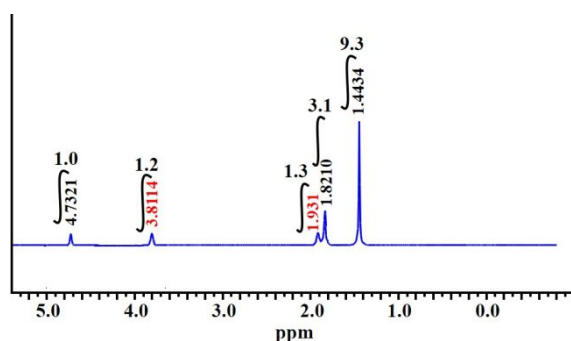


Fig. 3 ^1H NMR spectrum of heterometallic precursor $\text{Na}_2\text{Mg}_2(\text{tbaoc})_6(\text{THF})_2$ (**4**) in CDCl_3 recorded at room temperature.

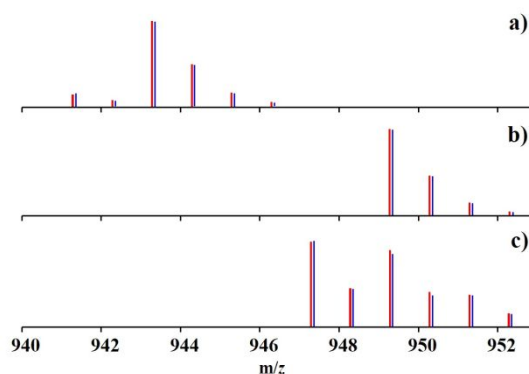


Fig. 4 Isotope distribution patterns for the $[\text{M-L}]^+$ ($L = \text{tbaoc}$) ion in positive ion DART mass spectra of precursors **1–3**: (a) $[\text{Na}_2\text{Fe}_2(\text{tbaoc})_5(\text{THF})_2]^+$, (b) $[\text{Na}_2\text{Co}_2(\text{tbaoc})_5(\text{THF})_2]^+$ and (c) $[\text{Na}_2\text{Ni}_2(\text{tbaoc})_5(\text{THF})_2]^+$. The blue and red lines are experimental and simulated patterns, respectively. Full analysis of mass spectra as well as the data for complex **4** can be found in ESI, Figs. S14–S17 and Tables S15–S26.

mass spectrometry, which was previously shown^{15,16,18} as very effective for the task due to its soft ionization process. In the positive ion spectra, the presence of the $[\text{M-L}]^+$ ions ($L = \text{tbaoc}$) for all molecular precursors was unambiguously confirmed along with their corresponding characteristic isotope distribution patterns (Fig. 4). Noteworthy is the observation that the $[\text{M-L-2THF}]^+$ species have also been detected, indicating the retention of heterometallic core with a proper $\text{Na}:\text{M} = 1:1$ ratio in the gas phase even upon dissociation of THF molecules (ESI, Figs. S14–S17).

Understanding the thermal behavior of heterometallic precursors is greatly important for the preparation of target oxide materials by thermal decomposition. Thermogravimetric analysis (TGA) of molecular precursor $\text{Na}_2\text{Fe}_2(\text{tbaoc})_6(\text{THF})_2$ (**1**) was carried out in the air to corroborate the visual and thermogravimetric observations of its behavior upon heating (ESI, Fig. S18). The obvious degradation of compound **1** starts at $50\text{--}60\text{ }^\circ\text{C}$ and is related to the departure of THF molecules. A fast weight loss takes place between $128\text{--}132\text{ }^\circ\text{C}$ and gradually ends at *ca.* $400\text{ }^\circ\text{C}$. The total weight loss at this point is 81.3%, which corresponds well to the theoretical value of 82.2% for the formation of stoichiometric target oxide NaFeO_2 . The next weight loss occurs above $700\text{ }^\circ\text{C}$ and is attributed to the slow evaporation of sodium in the form of oxide/peroxide. The total weight loss (88.3%) measured at $800\text{ }^\circ\text{C}$ may indicate the formation of Fe_2O_3 with a theoretical residue value of 87.2%.

Thermal decomposition of heterometallic single-source precursors **1–3** results in phase-pure oxides, which represent prospective cathode materials for the sodium-ion batteries. Specifically, phase-pure O'3-type NaNiO_2 was obtained through thermal decomposition of $\text{Na}_2\text{Ni}_2(\text{tbaoc})_6(\text{THF})_2$ (**3**) at $600\text{ }^\circ\text{C}$ (Fig. 5a, ESI, Fig. S23 and Table S31), while single-source precursors $\text{Na}_2\text{Fe}_2(\text{tbaoc})_6(\text{THF})_2$ (**1**) and $\text{Na}_2\text{Co}_2(\text{tbaoc})_6(\text{THF})_2$ (**2**) demonstrate versatility in preparation of different phases upon thermolysis at different temperatures/conditions (Fig. 5b and 5c). Low-temperature decomposition ($450\text{ }^\circ\text{C}$) of $\text{Na}_2\text{Fe}_2(\text{tbaoc})_6(\text{THF})_2$ (**1**) in O_2

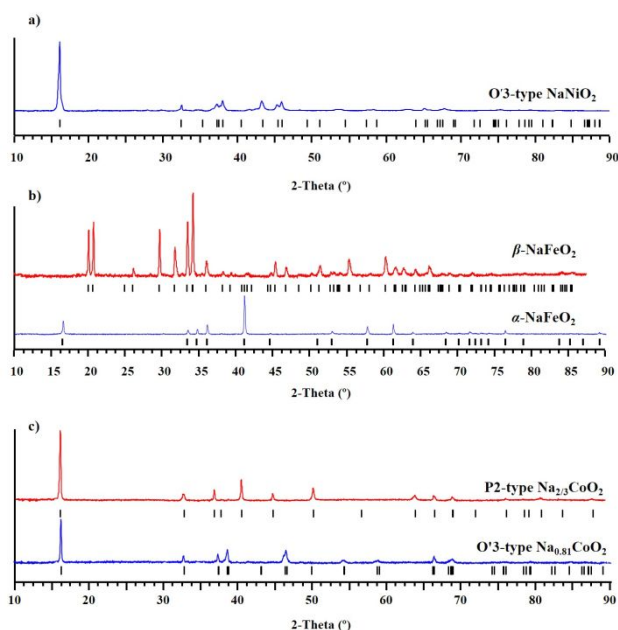


Fig. 5 X-ray powder diffraction patterns of (a) O'3-type of NaNiO_2 , (b) α (O3)- and β -types of NaFeO_2 , and (c) O'3- and P2-types of Na_xCoO_2 oxides obtained by thermal decomposition of respective single-source precursors under different conditions.

atmosphere results in stoichiometric α (O3)- NaFeO_2 phase, while treatment of **1** at 500 °C in air leads to a different polymorph, namely β - NaFeO_2 (Fig. 5b, ESI, Figs. S19 and S20, Tables S27 and S28). Thermal decomposition of $\text{Na}_2\text{Co}_2(\text{tbaaac})_6(\text{THF})_2$ (**2**) at relatively low-temperature (450 °C) yields O'3- Na_xCoO_2 phase, while elevating temperature to 750 °C gives rise to the P2-type of Na_xCoO_2 oxide (Fig. 5c, ESI, Figs. S21 and S22, Tables S29 and S30). Apparently, the thermolysis of compound **2** is accompanied by the gradual loss of sodium *via* its sublimation in the form of oxide/peroxide, which is a common phenomenon in the preparation of sodium-cobalt oxides.⁵ ICP analysis confirmed the Na:Co ratios in decomposition products as 0.81 and 0.70 for the O'3 and P2 forms, respectively, that corresponds well to the structural characteristics obtained by X-ray powder diffraction technique. Transmission electron microscopy (TEM) of P2- Na_xCoO_2 oxide obtained by thermal decomposition of molecular precursor **2** revealed the particles size in the range of 60–130 nm (ESI, Fig. S24a). The circular voltammetry and galvanostatic discharge behavior of this material has been briefly investigated. With Ag and Pt wires as the reference and counter electrodes, the P2- Na_xCoO_2 oxide is active within the potential range of -1.5–0.5 V (ESI, Fig. S24b) and the discharge capacities in the first two cycles reaching up to 124 and 128 mAh/g (ESI, Fig. S24c), respectively, which are superior to most of the data reported so far.^{1,3} However, a severe capacity fading starts afterward. This may be ascribed to the particle pulverization resulting from sodium ion intercalation during the first two reaction cycles.

In conclusion, the first series of heterometallic molecular precursors $\text{Na}_2\text{M}_2(\text{tbaaac})_6(\text{THF})_2$ were obtained. They all exhibit isomorphous tetranuclear structures with the Na:M

ratio of 1:1 and demonstrate clean decomposition patterns to yield phase-pure sodium-transition metal oxides, which belong to an important class of cathode materials for sodium-ion batteries. In addition to this application, the reported tetranuclear structure can be employed as a model for further design of heterotrimetallic $\text{Na}_2\text{MM}'(\text{tbaaac})_6(\text{THF})_2$ molecular precursors featuring two different 3d transition metal ions.

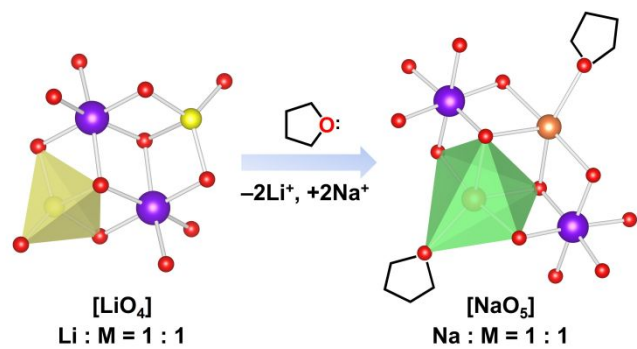
This work was financially supported by the National Science Foundation (CHE-1152441).

Conflicts of interest

There are no conflicts to declare.

Notes and references

1. N. Yabuuchi, K. Kubota, M. Dahbi and S. Komaba, *Chem. Rev.*, 2014, **114**, 11636–11682.
2. N. Yabuuchi and S. Komaba, *Sci. Technol. Adv. Mater.*, 2014, **15**, 043501–043529.
3. J.-Y. Hwang, S.-T. Myung and Y.-K. Sun, *Chem. Soc. Rev.*, 2017, **46**, 3529–3614.
4. C. Delmas, C. Fouassier and P. Hagenmuller, *Physica B+C*, 1980, **99**, 81–85.
5. M. Li, K. Yang, J. Liu, X. Hu, D. Kong, T. Liu, M. Zhang and F. Pan, *Chem. Commun.*, 2018, **54**, 10714–10717.
6. X. Ma, H. Chen and G. Ceder, *J. Electrochem. Soc.*, 2011, **158**, A1307–A1312.
7. N. K. Samin, R. Rusdi, N. Kamarudin and N. Kamarulzaman, *Adv. Mater. Res. (Durnten-Zurich, Switz.)*, 2012, **545**, 185–189.
8. P. Vassilaras, X. Ma, X. Li and G. Ceder, *J. Electrochem. Soc.*, 2013, **160**, A207–A211.
9. X. Wang, M. Tamaru, M. Okubo and A. Yamada, *J. Phys. Chem. C*, 2013, **117**, 15545–15551.
10. J. Billaud, R. J. Clément, A. R. Armstrong, J. Canales-Vázquez, P. Rozier, C. P. Grey and P. G. Bruce, *J. Am. Chem. Soc.*, 2014, **136**, 17243–17248.
11. S. Hildebrandt, A. Eva, P. Komissinskiy, C. Fasel, I. Fritsch and L. Alff, *J. Sol-Gel Sci. Technol.*, 2012, **63**, 307–314.
12. T. Kodera and T. Ogihara, *J. Ceram. Soc. Jpn.*, 2014, **122**, 483–487, 485 pp.
13. J. Zhao, J. Xu, D. H. Lee, N. Dimov, Y. S. Meng and S. Okada, *J. Power Sources*, 2014, **264**, 235–239.
14. A. Navulla, L. Huynh, Z. Wei, A. S. Filatov and E. V. Dikarev, *J. Am. Chem. Soc.*, 2012, **134**, 5762–5765.
15. H. Han, Z. Wei, M. C. Barry, A. S. Filatov and E. V. Dikarev, *Dalton Trans.*, 2017, **46**, 5644–5649.
16. H. Han, Z. Wei, M. C. Barry, J. C. Carozza, M. Alkan, A. Y. Rogachev, A. S. Filatov, A. M. Abakumov and E. V. Dikarev, *Chem. Sci.*, 2018, **9**, 4736–4745.
17. Z. Wei, H. Han, A. S. Filatov and E. V. Dikarev, *Chem. Sci.*, 2014, **5**, 813–818.
18. H. Han, Z. Wei, A. S. Filatov, J. C. Carozza, M. Alkan, A. Y. Rogachev, A. Shevtsov, Artem M. Abakumov, C. Pak, M. Shatruk, Y.-S. Chen and E. V. Dikarev, *Chem. Sci.*, 2019, **10**, 524–534.



Based on the $\text{Li}_2\text{M}_2\text{L}_6$ model structure, an addition of extra neutral donor ligand enables the formation of $\text{Na}_2\text{M}_2\text{L}_6(\text{THF})_2$ molecular precursors for the NaMO_2 oxide cathode materials.